

A search for high-redshift direct collapse black hole candidates in the PEARLS north ecliptic pole field

Armin Nabizadeh¹, Erik Zackrisson¹, Fabio Pacucci², Peter W. Maksym², Weihui Li¹, Francesca Civano², Seth H. Cohen³, Jordan C. J. D'Silva^{8,9}, Anton M. Koekemoer⁴, Jake Summers³, Rogier A. Windhorst³, Nathan Adams⁷, Christopher J. Conselice⁷, Dan Coe^{4,5,6}, Simon P. Driver⁸, Brenda Frye¹⁰, Norman A. Grogin⁴, Rolf A. Jansen³, Madeline A. Marshall^{11,9}, Mario Nonino¹², Nor Pirzkal⁴, Aaron Robotham⁸, Michael J. Rutkowski¹³, Russell E. Ryan, Jr.⁴, Scott Tompkins³, Christopher N. A. Willmer¹⁰, Haojing Yan¹⁴, Jose M. Diego^{15,16}, Cheng Cheng¹⁷, Steven L. Finkelstein¹⁸, S. P. Willner², Adi Zitrin¹⁹, Rachana Bhatawdekar²⁰, and Hansung B. Gim²¹

- ¹ Observational Astrophysics, Department of Physics and Astronomy, Uppsala University, Box 516, SE-751 20 Uppsala, Sweden
e-mail: armin.nabizade@gmail.com
- ² Center for Astrophysics | Harvard & Smithsonian, 60 Garden St., Cambridge, MA 02138, USA
- ³ School of Earth and Space Exploration, Arizona State University, Tempe, AZ 85287-1404
- ⁴ Space Telescope Science Institute, 3700 San Martin Drive, Baltimore, MD 21218, USA
- ⁵ Association of Universities for Research in Astronomy (AURA) for the European Space Agency (ESA), STScI, Baltimore, MD 21218, USA
- ⁶ Department of Physics, 366 Physics North MC 7300, University of California, Berkeley, CA 94720, USA
- ⁷ Jodrell Bank Centre for Astrophysics, Alan Turing Building, University of Manchester, Oxford Road, Manchester M13 9PL, UK
- ⁸ International Centre for Radio Astronomy Research (ICRAR) and the International Space Centre (ISC), The University of Western Australia, M468, 35 Stirling Highway, Crawley, WA 6009, Australia
- ⁹ ARC Centre of Excellence for All Sky Astrophysics in 3 Dimensions (ASTRO 3D), Australia
- ¹⁰ Steward Observatory, University of Arizona, 933 N Cherry Ave, Tucson, AZ, 85721-0009, USA
- ¹¹ National Research Council of Canada, Herzberg Astronomy & Astrophysics Research Centre, 5071 West Saanich Road, Victoria, BC V9E 2E7, Canada
- ¹² INAF-Osservatorio Astronomico di Trieste, Via Bazzoni 2, 34124 Trieste, Italy
- ¹³ Minnesota State University-Mankato, Telescope Science Institute, TN141, Mankato MN 56001, USA
- ¹⁴ Department of Physics and Astronomy, University of Missouri, Columbia, MO 65211, USA
- ¹⁵ Instituto de Física de Cantabria, Edificio Juan Jordá, Avenida de los Castros s/n, E-39005 Santander, Cantabria, Spain
- ¹⁶ Instituto de Física de Cantabria (CSIC-UC). Avenida. Los Castros, s/n. E-39005 Santander, Spain
- ¹⁷ Chinese Academy of Sciences, National Astronomical Observatories, CAS, Beijing 100101, People's Republic of China
- ¹⁸ Department of Astronomy, The University of Texas at Austin, 2515 Speedway, Stop C1400, Austin, Texas 78712, USA
- ¹⁹ Physics Department, Ben-Gurion University of the Negev, P.O. Box 653, Beer-Sheva 8410501, Israel
- ²⁰ European Space Agency (ESA), European Space Astronomy Centre (ESAC), Camino Bajo del Castillo s/n, 28692 Villanueva de la Cañada, Madrid, Spain
- ²¹ Department of Physics, Montana State University, P. O. Box 173840, Bozeman, MT 59717, USA

2023

ABSTRACT

Direct-collapse black holes (DCBHs) of mass $\sim 10^4\text{--}10^5 M_\odot$ that form in HI-cooling halos in the early Universe are promising progenitors of the $\gtrsim 10^9 M_\odot$ supermassive black holes that fuel the observed $z \gtrsim 7$ quasars. Efficient accretion of the surrounding gas onto such DCBH seeds may render them sufficiently bright for detection with the James Webb Space Telescope (JWST) up to $z \approx 15$. Additionally, the very steep and red spectral slope predicted across the $\approx 1\text{--}5 \mu\text{m}$ wavelength range of the JWST/NIRSpec instrument during their initial growth phase should make them photometrically identifiable up to very high redshifts. Here, we present a search for such DCBH candidates across the 34 arcmin² in the first two spokes of the JWST cycle-1 "Prime Extragalactic Areas for Reionization and Lensing Science" (PEARLS) survey of the North Ecliptic Pole Time Domain Field (NEP), covering 8 NIRCам filters down to a maximum depth of ~ 29 AB mag. We identify three objects with spectral energy distributions consistent with the Pacucci et al. (2016) DCBH models. However, we also note that even with data in 8 NIRCам filters, objects of this type remain degenerate with dusty galaxies and obscured active galactic nuclei over a wide range of redshifts. Follow-up spectroscopy would be required to pin down the nature of these objects, and two of our DCBH candidates are sufficiently bright to make this practical. Based on our sample of DCBH candidates and assumptions on the typical duration of the DCBH steep-slope state, we set a conservative upper limit of $\approx 7 \times 10^{-4}$ comoving Mpc⁻³ (cMpc⁻³) on the comoving density of host halos capable of hosting DCBHs with spectral energy distributions similar to the Pacucci et al. (2016) models at $z \approx 6\text{--}13$.

Key words. Quasars: supermassive black holes – Stars: black holes – Stars: Population III – Infrared: general – Cosmology: early Universe

1. Introduction

In the history of the Universe, the evolution of galaxies and supermassive black holes (SMBHs) is tightly connected. More than 200 quasars powered by SMBHs of mass $\gtrsim 10^9 M_\odot$ are now discovered at redshift $z \gtrsim 6$ (e.g. Fan et al. 2001, 2003; Mortlock et al. 2011; Wu et al. 2015; Bañados et al. 2018; Yang et al. 2020; Wang et al. 2021; Fan et al. 2022), with some of them shining when the age of the Universe was less than 800 Myr. Explaining how black holes reach such masses this early in the history of the Universe is challenging and requires some combination of highly efficient gas accretion and black hole mergers (Pacucci & Loeb 2020) starting from lower mass ($\sim 10^2$ – $10^6 M_\odot$) black hole seeds (see, e.g., Woods et al. 2019; Inayoshi et al. 2020; Fan et al. 2022, for recent reviews). Thus, the discovery of high-redshift SMBHs is instrumental in constraining the properties of the seed population of black holes (Pacucci & Loeb 2022).

Several formation mechanisms for such seeds are proposed in the literature: (i) primordial formation during inflation or from cosmic string loops (e.g., Hasinger 2020); (ii) formation as the end product of massive and metal-free stars, possibly undergoing super-Eddington accretion episodes (e.g. Begelman 1978; Wyithe & Loeb 2012; Begelman & Volonteri 2017); (iii) formation through runaway stellar mergers in young star clusters (e.g. Portegies Zwart & McMillan 2002; Davies et al. 2011; Katz et al. 2015; Boekholt et al. 2018); and (iv) formation via direct-collapse black holes (DCBHs; Loeb & Rasio 1994; Bromm & Loeb 2003; Lodato & Natarajan 2006; Pacucci et al. 2017a; Inayoshi et al. 2020; Volonteri et al. 2021).

In the DCBH scenario, gas within an atomic-cooling halo (i.e., $\gtrsim 10^7 M_\odot$) collapses to form a $\sim 10^4$ – $10^6 M_\odot$ (Ferrara et al. 2014) black hole at $z \sim 20$ – 30 (e.g. Loeb & Rasio 1994; Bromm & Loeb 2003; Lodato & Natarajan 2006), possibly with a supermassive star or a quasi-star formed as an intermediate step (see Woods et al. 2019, for a review). Accretion onto the newly formed seed black hole from the surrounding gas, in duty cycles with active phases lasting up to ≈ 100 Myr (e.g. Pacucci et al. 2015), could render such DCBH sufficiently luminous to allow detection at $z > 7$, either in the near-to-mid infrared (IR) or in the X-ray regime. The high-energy emission is more sensitive to details of the accretion process, such as the gas metallicity and column density of the host galaxy (Pacucci et al. 2015, 2016). Current X-ray observatories, such as Chandra, have deep-field sensitivity limits of $\sim 10^{-17}$ erg s $^{-1}$ cm $^{-2}$, which render most of the seed population undetectable. Proposed X-ray probe-class missions, such as AXIS, could reach sensitivities of $\sim 10^{-18}$ erg s $^{-1}$ cm $^{-2}$ in their deep fields, allowing to uncover at least part of the population of seeds, especially in the heavy regime. In the deepest James Webb Space Telescope (JWST) exposures, DCBHs of initial mass $\sim 10^3 M_\odot$ may remain detectable up to $z \approx 20$ (Natarajan et al. 2017; Whalen et al. 2020), if supplied with large accretion rates from their host.

The likely observable signatures of DCBHs through JWST observations vary significantly, largely depending on the following factors (Pacucci et al. 2015, 2016; Natarajan et al. 2017; Valiante et al. 2017; Visbal & Haiman 2018; Valiante et al. 2018; Whalen et al. 2020; Inayoshi et al. 2022a; Nakajima & Maiolino 2022): (i) the evolutionary state of these objects, including factors such as the initial seed mass, gas density and metallicity of the host, and gas availability; (ii) the details of the accretion process onto the seed (e.g., the geometry of the disk and its radiative efficiency); (iii) the triggering of star formation in the host, possibly enhanced by soft X-ray irradiation from the DCBHs; (iv) and the merger history of DCBHs after formation.

Some models suggest that the light from the DCBH is likely to be blended with that of surrounding stars and associated nebular emission (Natarajan et al. 2017). This occurs either because the DCBH forms in the direct vicinity of star-forming halos (which provides the radiation required to deplete molecules in the DCBH host and prevent cooling) and merges with these on timescales as short as ~ 1 Myr (e.g. Pacucci et al. 2017a; Natarajan et al. 2017), or because star formation occurs within the DCBH host halo itself (e.g. Aykutalp et al. 2014; Valiante et al. 2018; Barrow et al. 2018; Aykutalp et al. 2020). In other scenarios, the DCBH can remain isolated for prolonged periods while efficiently growing in mass due to cold accretion (Whalen et al. 2020; Latif et al. 2022).

Consequently, the anticipated photometric spectral energy distributions (SEDs) of high-redshift DCBHs, spanning the wavelength range probed by JWST, exhibit a spectrum ranging from blue (e.g. Valiante et al. 2018; Barrow et al. 2018) to red (e.g. Pacucci et al. 2016; Whalen et al. 2020; Inayoshi et al. 2022b). The predicted formation rates of DCBHs as a function of redshift are also highly variable, mainly due to uncertainties in the level of background radiation necessary to prevent star formation and the effect of supernova feedback (Habouzit et al. 2016a). Theoretical predictions on the comoving number densities of halos capable of hosting DCBHs span $\gtrsim 5$ orders of magnitude at any given redshift (Habouzit et al. 2016a; Valiante et al. 2017), rendering estimates of DCBH detectability with JWST highly uncertain (e.g., Pacucci et al. 2019).

This work presents a photometric search for $z \gtrsim 6$ DCBH candidates in the PEARLS NEP field for which auxiliary X-ray data is available. In particular, we focus on the predictions of Pacucci et al. (2016), in which DCBHs, at birth, exhibit very steep (i.e., "red") SEDs within the wavelength range ≈ 1 – $5 \mu\text{m}$ probed by JWST/NIRCam. These SED models allow us to efficiently sift out promising candidates with current JWST observations because of the large slope in the near-to-mid IR.

A previous search by Pacucci et al. (2016) for such red DCBH candidates at $z \lesssim 10$ using data from the Hubble Space Telescope (HST), Spitzer, and Chandra revealed that objects at $H < 27$ AB mag exhibiting the relevant ≈ 1 – $5 \mu\text{m}$ signatures of $\sim 10^4$ – $10^6 M_\odot$ DCBHs do exist, but are very rare. However, this candidate selection was based on three broadband filters only in the range of 1 – $5 \mu\text{m}$. Given the superior depth and more diverse set of photometric filters provided by JWST, it remains unclear how many such candidates will remain consistent with a DCBH interpretation for further scrutiny.

The current work is organized as follows. In Section 2, we present the PEARLS data used, while Section 3 describes the selection criteria upon which our search is based. In Section 4, we present our main results: our DCBH candidates and the inferred upper limits on the comoving number density of DCBH host halos. Our findings are discussed and summarized in Section 5.

2. JWST/NIRCam data on the NEP field

The IR observations analyzed in this study were provided as a part of the Prime Extragalactic Areas for Reionization and Lensing Science" (PEARLS; PI: R. Windhorst; Windhorst et al. 2023) Guaranteed Time Observations (GTO) program. PEARLS is a time-domain survey of the North Ecliptic Pole (NEP) field which is being carried out in four "spokes" (Jansen & Windhorst 2018) covering a total survey area of 68 arcmin 2 (i.e., 17 arcmin 2 for each spoke as a 2×1 mosaic layout of NIRCam modules A and B; Rieke et al. 2023). The NEP Time-Domain Field, centered

at RA 17:22:47.896 and Dec +65:49:21.54, is within the JWST continuous viewing zone and has been imaged by NIRCcam in 8 near-IR bands using four short-wavelength (SW) filters (F090W, F115W, F150W, F200W), and four long-wavelength (LW) filters (F277W, F356W, F410M and 444W) with 5σ detection limits at 28–29 AB mag. The auxiliary data for this field contains the observations from the radio to X-ray (see Windhorst et al. 2023, for additional details). Here, we use spoke 1 and spoke 2 data catalogs covering a total area of 34 arcmin², and including ≈ 24120 objects.

The catalogs were created following the methodology outlined in Windhorst et al. (2023), with the only significant difference being the retention of point sources, as it is possible that DCBHs may remain unresolved. In a nutshell, Source Extractor (Bertin & Arnouts 1996) was utilized for source detection on 30 milli-arcsecond pixel-scale mosaics, astrometrically aligned to Gaia DR3, employing weight maps to aid in detection and account for flux uncertainties. Dual-image mode was employed, with the F444W image used for source detection and aperture definition. The minimum threshold for analysis and detection was set at 1.5σ in 9 connected pixels, while the deblending contrast parameter was set to 0.06 to strike a balance between completeness and reliability. All measured fluxes used Source Extractor's "automatic" apertures (i.e., *MAG_AUTO*).

Additionally, another remarkably important dataset in our search for $z > 6$ DCBH candidates is the *NuSTAR* 3–24 keV and *Chandra* 0.2–10 keV X-ray observations to select X-ray bright candidates (see Sec. 4.3).

3. Photometric signatures of direct-collapse black holes at $z \gtrsim 6$

High-redshift, accreting DCBHs that are surrounded by a sufficiently dense reservoir of gas, are Compton-thick (i.e., with a column density $n_H > 1.5 \times 10^{24} \text{ cm}^{-2}$) and can display a very red SED for prolonged periods of time at rest-frame ultraviolet and optical wavelengths (Pacucci et al. 2016). This serves as a photometric signature across the 1–5 μm range probed by JWST/NIRCcam at $z \gtrsim 6$. In this phase of evolution, the DCBH may also be detectable in the X-ray regime, although the X-ray flux is highly model-dependent and can lie below the detection threshold of all current X-ray telescopes (Pacucci et al. 2015), except during the brightest phases of accretion.

In Figure 1, we plot the SED of the Pacucci et al. (2016) $5 \times 10^6 M_\odot$ DCBH model at $z = 6$ –20 against the PEARLS JWST/NIRCcam detection limits. As seen, this model remains detectable in at least 4 JWST/NIRCcam filters until $z = 20$ and displays a very red spectral slope.

While this significantly red SED ensures that DCBHs stand out from the majority of $z \gtrsim 6$ objects, it also presents a number of challenges. The intrinsically red slope of the SED can, in fact, make it difficult to assess the wavelength of the Lyman- α ($\text{Ly}\alpha$) break, since the flux in the filter covering wavelengths directly longward of the "dropout" filter may also fall below the detection threshold in the case of faint DCBHs. As a reminder, the $\text{Ly}\alpha$ break renders the flux at wavelengths $\lesssim 0.1216(1+z) \mu\text{m}$ undetectably low due to absorption in the neutral intergalactic medium for light sources at $z \gtrsim 6$, and is often used to determine the redshift. The situation is illustrated in Figure 2, where we show that DCBHs over a relatively large redshift range ($\Delta z \approx 4$) can produce photometric SEDs that are observationally indistinguishable given the NEP detection limit.

A second challenge comes from the fact that the relatively featureless photometric SEDs of the Pacucci et al. (2016)

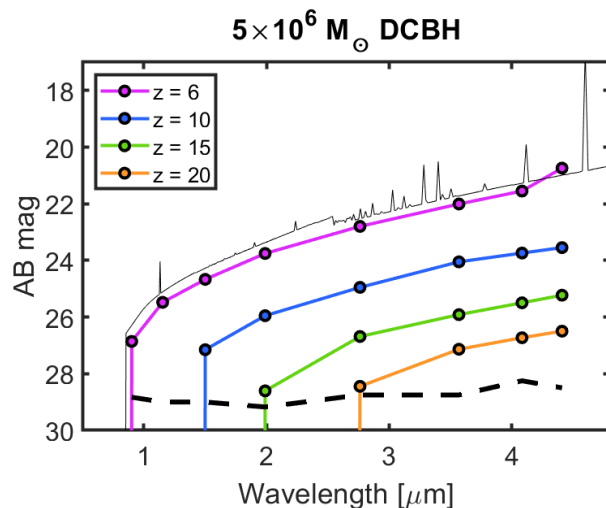


Fig. 1. DCBH detection limits in the NEP. The dashed thick line represents the combined JWST/NIRCcam 5σ flux detection limits expressed in AB magnitudes across the NEP spokes. The colored lines show the photometric fluxes of the Pacucci et al. (2016) $5 \times 10^6 M_\odot$ DCBH model at $z = 6, 10, 15$, and 20 , in the set of NIRCcam filters used by PEARLS across the NEP field. The thin black solid line shows the $z = 6$ version of the DCBH model spectrum on which the photometric predictions are based, but offset by 0.5 magnitudes for clarity. As seen, this Pacucci et al. (2016) $5 \times 10^6 M_\odot$ DCBH model remains detectable up to $z = 20$ in the reddest NIRCcam filters used. The photometric SEDs are characterized by a significantly red slope across the NIRCcam bands and are relatively featureless except for the drop at the $\text{Ly}\alpha$ limit and the bump seen in the F444W filter at $z = 6$ SED, which is due to strong $\text{H}\alpha$ emission. This is not seen in the higher-redshift SEDs, since it redshifts out of the NIRCcam range at $z \gtrsim 6.9$.

DCBHs may be confused with other rare types of objects. Low-temperature stars or substellar objects in the Milky Way could appear as very red point sources and in some cases potentially be confused with compact objects at high redshifts. However, the detailed JWST/NIRSpec SEDs of our DCBH models at $z = 5$ –20 do not match the SEDs of any of the faint star or brown dwarf models in the sets of Baraffe et al. (2015) and Phillips et al. (2020), and such objects are therefore unlikely to be confused with DCBHs in the current search. Dusty galaxies and obscured AGN are far more likely interlopers, and in Fig. 3 we show that—even when imaging in 8 NIRCcam filters is available—the photometric signatures of DCBHs may be reproduced by both of these types of objects. When only parts of the NIRCcam wavelength range are probed (i.e., when colors featuring just a few of the NIRCcam wide-band filters are used as diagnostics), DCBHs may also display similar colors as some of the very reddest objects detected so far by JWST, including AGN candidates and so-called HST-dark galaxies (Rodighiero et al. 2023; Furtak et al. 2022; Larson et al. 2023; Barrufet et al. 2023; Kokorev et al. 2023; Barro et al. 2023; Matthee et al. 2023; Labbe et al. 2023; Smail et al. 2023). For example, Kocevski et al. (2023) has reported on the discovery of a broad-line AGN at $z \approx 5.6$ which at ≈ 2 –4.4 μm displays a steep/red SED very similar to our DCBH models, whereas the ≈ 1.15 –1.5 part is relatively flat in f_ν units (many similar SEDs are also seen in Barro et al. 2023; Labbe et al. 2023). In its entirety, this type of SED would not allow a good fit to our DCBH models, but if the source had been intrinsically fainter so that the short-wavelength part had fallen placed

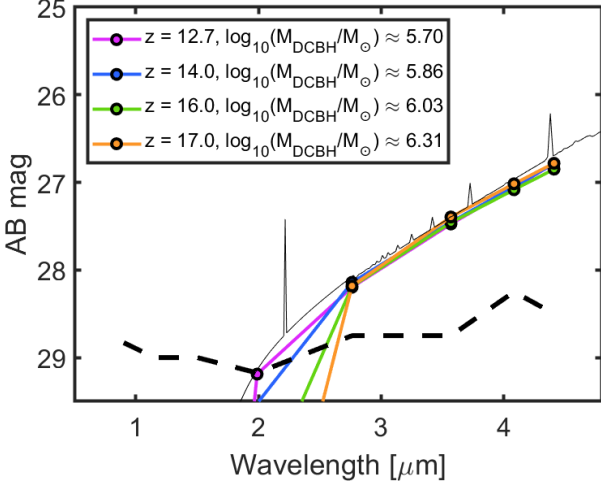


Fig. 2. The mass-redshift degeneracy for DCBH SEDs without a clear-cut Ly α break. If the Ly α break is close to or below the detection threshold (dashed black line), acceptable SED fits to NIRCcam data at longer wavelengths can be achieved for DCBH models over a wide range of redshifts. Here, the purple line corresponds to the photometric SED of a $z = 12.7$ DCBH with mass $\log_{10}(M_{\text{DCBH}}/M_{\odot}) \approx 5.70$ and the thin solid line is the corresponding spectrum (offset by 0.1 magnitudes for clarity). In this case, the Ly α break occurs at $\approx 1.7 \mu\text{m}$, in between the F150W and F200W filters. While the F200W flux is largely unaffected by the Ly α break, the red slope of the DCBH SED still places the F200W flux below the detection limit of the NEP field (black dashed line). Since a sharp drop in flux at the Ly α limit becomes unobservable in this case, the redshift becomes poorly constrained as higher-mass DCBH models at $z = 14$ (blue line), $z = 16$ (green line) and $z = 17$ (orange line) produce very similar fluxes in the longer-wavelength NIRCcam filters (F277W, F356W, F410M, and F444W).

below the detection threshold, our search procedure would likely have identified this SED as a likely DCBH.

This means that all photometrically selected DCBH candidates should be considered tentative until confirmed through spectroscopy, as discussed in Section 5. In Appendix A, we provide some further exploration of the properties of galaxies capable of mimicking the SEDs of DCBHs.

4. DCBH candidates

To produce a grid of SED models for DCBHs against which the objects in the PEARLS/NEP catalogs are tested, we started from the Pacucci et al. (2016) models of a DCBH with seed mass around $10^5 M_{\odot}$, and extracted SEDs at times where the black hole mass has grown to $M_{\text{DCBH}} = 5 \times 10^5$, 1×10^6 , 5×10^6 and $7 \times 10^6 M_{\odot}$. These original four DCBH model spectra were then interpolated to form 50 DCBH spectra uniformly spaced in $\log_{10} M_{\text{DCBH}}$ throughout the 5×10^5 – $7 \times 10^6 M_{\odot}$ range. On this basis, we derived photometric fluxes in the relevant NIRCcam filters at $z = 5$ – 15 with a step size of $\Delta(z) = 0.1$. We assumed a cosmology characterized by $\Omega_M = 0.32$, $\Omega_{\Lambda} = 0.68$, and $H_0 = 67 \text{ km s}^{-1} \text{ Mpc}^{-1}$, as well as complete absorption by the neutral intergalactic medium at rest wavelengths shorter than Ly α for sources at $z > 5.8$.

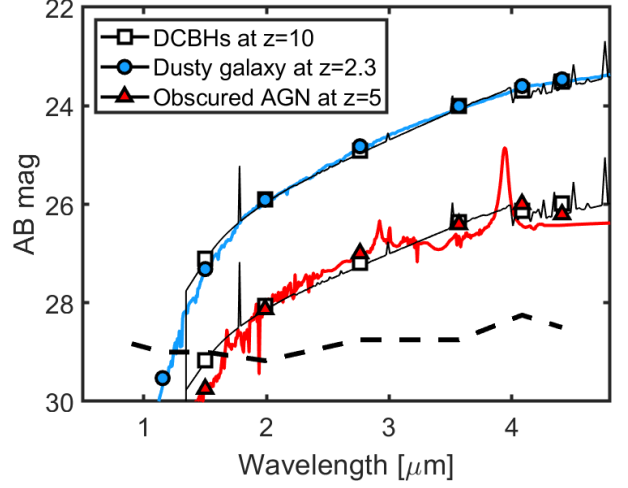


Fig. 3. The photometric degeneracy between high- z DCBHs, obscured AGN and very dusty galaxies. The black thin lines represent the Pacucci et al. (2016) model spectra of DCBHs with mass $5 \times 10^6 M_{\odot}$ (upper line) and $5 \times 10^5 M_{\odot}$ (lower line) at $z = 10$. The white squares indicate the corresponding integrated fluxes in the NIRCcam filters used in the PEARLS/NEP survey. While the detailed spectra of DCBHs display features that would set them apart from both dusty galaxies and obscured AGN, their photometric properties can be relatively well reproduced by both of these types of objects. The blue line represents the model spectrum of a passively evolving, very dusty ($A_V \approx 2.5 \text{ mag}$, $Z = 0.004$, age $\approx 2 \text{ Gyr}$) galaxy at $z = 2.3$ based on the Zackrisson et al. (2011b) set, with filter fluxes (blue squares) that can roughly reproduce the photometric data points of the $5 \times 10^6 M_{\odot}$ DCBH that lie above the PEARLS/NEP detection threshold (black dashed line). The red line and red triangles represent the Polletta et al. (2007) template spectrum and its corresponding NIRCcam filter fluxes for an obscured AGN (QSO2 template), redshifted to $z = 5$ and scaled to match the $5 \times 10^5 M_{\odot}$ DCBH model as closely as possible. Also in this case, there is a substantial similarity in the photometric SED between the $z = 5$ AGN and the $z = 10$ DCBH.

4.1. DCBH candidate selection

The search for potential DCBH candidates among the 24,119 objects listed in PEARLS/NEP1+NEP2 catalog began by selecting those observations with at least four detected fluxes above the JWST NIRCcam 5σ detection limit (see Sec. 2). For fluxes associated with unrealistically small error bars, such as $< 0.1 \text{ mag}$, we capped both upper and lower error bars at 0.1 mag . SED fitting using reduced- χ^2 (χ^2_{ν}) minimization was then performed for every catalog object using all the Pacucci et al. (2016) DCBH models described above. Consequently, three sources with IDs 21567, 22802, and 14830 revealed acceptable fits with $\chi^2_{\nu} < 3$ — from now on, we refer to the three DCBH candidates as DCBH-1, DCBH-2, and DCBH-3, designated in arbitrary order. Based on the minimum and maximum degrees of freedom (2 and 6), the corresponding limits of the P-values for the selected χ^2_{ν} range are 0.049 and 0.006. Therefore, considering a maximum χ^2_{ν} of 3 is quite generous for this analysis and ensures that the upper limits on the comoving density of DCBH host halos in Section 4.2 are conservative. The fit parameters and the source information of all detections are listed in Table 1. In the case of DCBH-3, we note that despite the absence of any detectable source in the F090 filter image, there is a faint flux reported in the catalog for this filter. Therefore, we have retained the source in the list as its value falls below the 5σ detection limit. This observation

could potentially be attributed to the automated source detection employed as part of the data reduction procedure. These three candidates are deemed suitable for follow-up spectroscopy due to their high brightness and relatively high signal-to-noise ratios. Thumbnail images and SED fits of these three candidates are shown in Figure 4.

As expected, the photometric SEDs exhibit extremely red continuum slopes through the NIRCcam bands. At the flux levels of these candidates, the first data point at wavelengths longward of the Ly α limit lies too close to the NEP detection threshold to allow a sharp Ly α limit feature to be seen (unlike in the $z = 6$ and $z = 10$ examples shown in Figure 1). Instead, the continuum gradually fades below the detection limit, which, unfortunately, makes the redshift difficult to constrain. These photometric signatures may also be reproduced by obscured AGN or very dusty galaxies (see Sec. 3 and Fig. A.1).

We note that there is a range of morphologies among these sources, with two of the candidates being extended and one more point-like. Naively, one would expect DCBHs to appear as unresolved point sources, but the presence of ionized gas surrounding the DCBH or/and its proximity to a nearby galaxy could also be consistent with an extended source. However, it is important to note that if the extended source is indeed a galaxy, the Pacucci et al. (2016) DCBH SED fitting method will not yield accurate results.

4.2. The comoving density of direct collapse black holes

The prospects of detecting DCBHs in a given survey are set by a combination of two factors: (i) the flux detection limits of the photometric and/or spectroscopic observations used, and (ii) the sky area covered by this survey. Whereas the flux detection thresholds set limits on the properties of the observable DCBHs (in terms of black hole mass, accretion rate, etc.), the survey area determines the number of such objects that are included in the survey.

The connection between the survey area and the expected number of DCBH detections is further complicated by substantial uncertainties regarding the properties required for DCBHs to form. Theoretical predictions on the number density of halos that could host DCBHs at $z = 6$ –20 spans at least five orders of magnitude at any given redshift (Habouzit et al. 2016b; Valiante et al. 2017; Inayoshi et al. 2020).

To compare current predictions on the number density of DCBH host halos to the number density that would allow at least one detection in PEARLS, we derived the comoving number density n_{hosts} of host halos that would produce a certain number of observed DCBH candidates (N_{obs}) in the $\Delta(z)$ interval centered around redshift z as:

$$n_{\text{hosts}} = \frac{N_{\text{obs}}}{V_c(A, z, \Delta(z)) \Delta t_{\text{DCBH}}}, \quad (1)$$

where $V_c(A, z, \Delta(z))$ is the comoving volume probed by a survey that covers an area A in the sky across $\Delta(z)$ at redshift z , $\Delta t_{z, \Delta(z)}$ is the cosmic time interval spanned by $\Delta(z)$ at this redshift and Δt_{DCBH} is the total time interval during which a DCBH can be expected to exhibit some specific set of selection criteria. In the case of the NEP, we based the $V_c(A, z, \Delta(z))$ estimate on a survey area for two spokes (see below).

By requiring DCBH candidates to be detectable in at least four JWST/NIRCcam filters, the maximum redshift for which DCBHs may be detected throughout the full $0.5 - 7 \times 10^6 M_{\odot}$ mass range considered corresponds to $z \approx 13$ when using

PEARLS data for the NEP field. By comparison, other JWST cycle-1 surveys like the Cosmic Evolution Early Release Science (CEERS¹; $\approx 100 \text{ arcmin}^2$ in the Extended Groth Strip; Finkelstein et al. 2022) and JWST Advanced Deep Extragalactic Survey (JADES²; $\approx 175 \text{ arcmin}^2$ in GOODS-S and GOODS-N; Eisenstein et al. 2023) with somewhat deeper detection limits have the potential to extend this limit to $z = 16$ and 17, respectively.

By setting $N_{\text{obs}} = 1$ in equation 1, Fig. 5 displays the minimum DCBH host halo number densities detectable in PEARLS-NEP, CEERS, and JADES as a function of redshift under the assumption that $0.5 - 7 \times 10^6 M_{\odot}$ DCBHs retain their Pacucci et al. (2016) tell-tale spectral signatures for $\Delta t_{\text{DCBH}} = 10 \text{ Myr}$.

These detection limits were compared to the range of theoretical predictions on the comoving number densities of DCBH hosts from Habouzit et al. (2016b). DCBH models that fall above these limits could produce DCBH detections within the specified survey areas, whereas models falling below would produce too few DCBHs per comoving volume to make detections likely.

Based on our analysis using PEARLS NEP1 and NEP2 observations, we found three potential sources at different redshifts (see 4.1 for details). Assuming $N_{\text{obs}} = 3$ and the PEARLS survey area of $\sim 34 \text{ arcmin}^2$ for two spokes, the upper limit on the comoving density of host halos that host DCBHs that have grown to $5 \times 10^5 - 7 \times 10^7 M_{\odot}$ and exhibit SEDs in accord with the Pacucci et al. (2016) models then becomes $\approx 2 - 7 \times 10^{-4} \text{ cMpc}^{-3}$ ("c" stands for co-moving density; lower part of dark grey region in Fig. 5) at $z = 6$ –13. These limits are conservative since they are derived under the assumption that all candidates potentially could be at the same redshift. We stress that the redshift estimates for the candidates, obtained by Pacucci et al. (2016), are photometric and therefore subject to substantial uncertainties (as also discussed in Section 3).

These limits already exclude the upper part of the Habouzit et al. (2016b) parameter space at these redshifts. By increasing the timescale over which DCBHs are detectable to 100 Myr, both the upper limit and the theoretical detection limits of the various surveys would shift downward by one dex in this diagram.

Since the predicted range of host number densities extends well above the detection limits of PEARLS/NEP, CEERS, and JADES, DCBH detections may be possible even if a small fraction of potential DCBH host halos would produce sources with the spectral characteristics we use for candidate selection. However, since the predicted range also extends below the detection limits, success in detecting DCBHs in these JWST surveys is not assured. In Fig. 5, we considered only number densities from the Habouzit et al. (2016b) simulation scenarios that successfully generate DCBH candidate halos—not the Habouzit et al. (2016b) simulation scenarios that failed to produce any such objects within the simulated volume. If the latter actually provides better representations of reality, then the DCBH number density could in principle be even lower than that shown in Fig. 5.

However, if DCBHs serve as the primary seeds of early SMBHs, a hard lower limit can be set by considering the comoving number densities of $z \approx 6$ quasars ($\sim 10^{-9} \text{ cMpc}^{-3}$; e.g., Valiante et al. 2017), since the DCBH host halo number density must then exceed this limit at some prior redshift. As the area-based detection limits are shown for $z = 6$ –13, we stress that specific DCBH models (originally obtained in the range $z = 6$ –20) may not have the properties required for detection and identifica-

¹ <https://ceers.github.io>

² <https://www.cosmos.esa.int/web/jwst-nirspec-gto/jades>

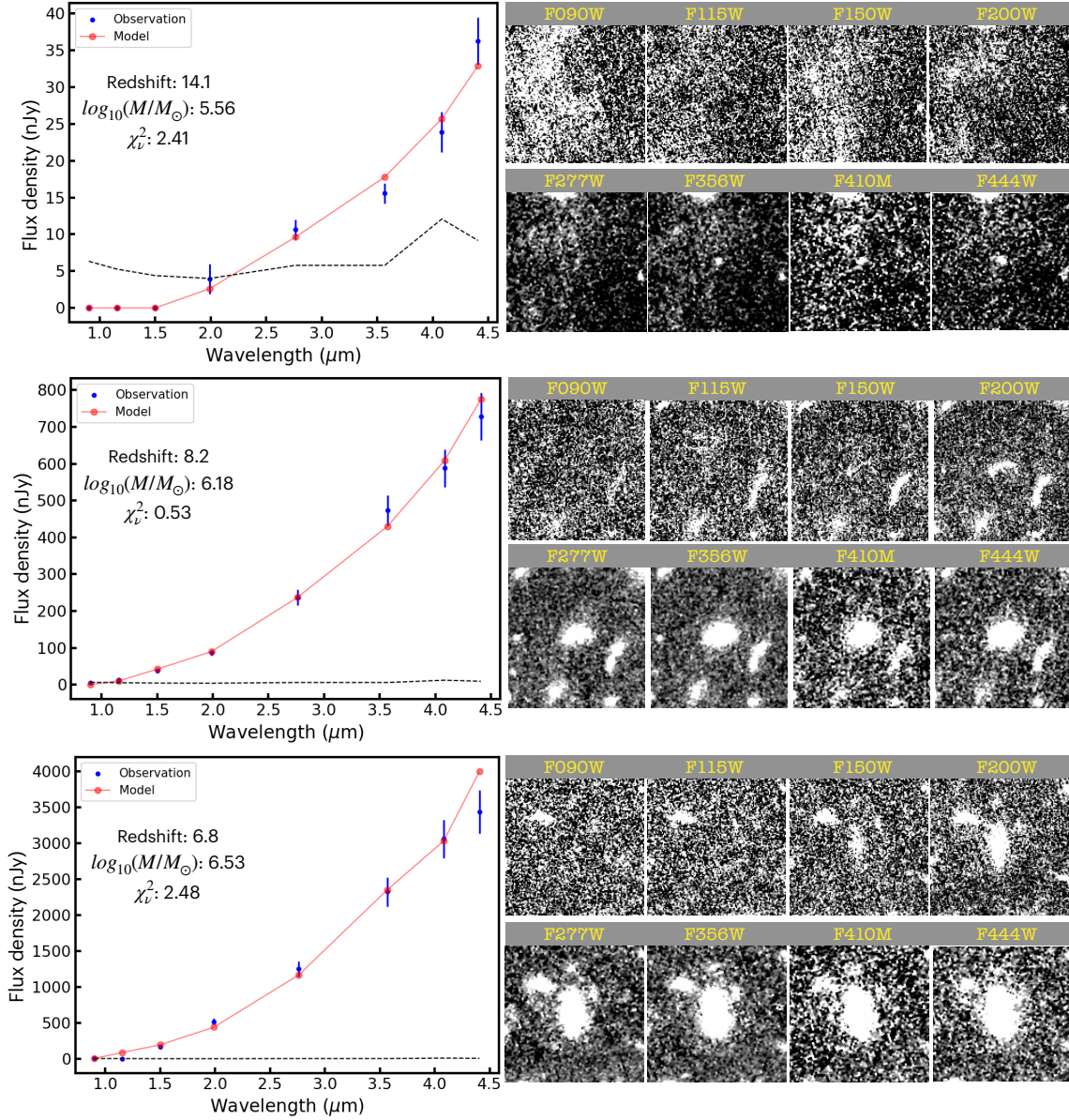


Fig. 4. DCBH candidates in PEARLS/NEP. In the left column, we show the JWST/NIRCam photometric fluxes in 8 bands (blue dots) and the corresponding best-fitted photometric DCBH models (red dots and solid line) from Pacucci et al. (2016). The dashed lines correspond to NIRCам detection limits. In the right columns, we show the corresponding 2 × 2 arcsec images for objects DCBH-1 (top), DCBH-2 (middle), and DCBH-3 (bottom). Tabulated fluxes and coordinates of these objects are listed in Table 1.

tion at all of these redshifts. Consequently, taking the PEARLS detection limit, the highest redshift in which a DCBH can be detected in the mass range $0.5 - 7 \times 10^6$ is $z = 13$.

4.3. Constraints on X-ray emission

In order to constrain the X-ray emission of our three candidates (see Fig. 4), we used the 1.3 megaseconds *Chandra* observations available in the field. By using different extraction regions centered at each source position (the 50% encircled energy, 0.32 arcsec in all cases, and $r = 1$ arcsec) and 3"–5" annulus for background extraction, we obtain non-detections for all three candidates. In this case, we can compute 3σ upper limits on count rates of $1.7 \times 10^{-6} \text{ count s}^{-1}$, which translates to an upper limit on the observed flux of $\sim 3 \times 10^{-17} \text{ erg s}^{-1} \text{ cm}^{-2}$ in the 0.5–7 keV band assuming a power-law model with spectral

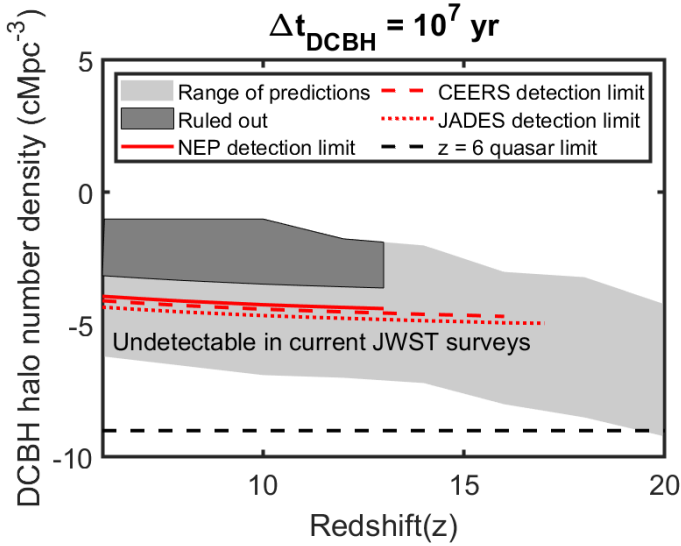
index of $\Gamma = 1.4$. This flux translates into an X-ray luminosity of $\sim 7 \times 10^{43}$ in the 0.5–7 keV band at redshift $z = 7$. The *XMM-Newton* and *NuSTAR* data available in this field (Zhao et al. 2021) were also searched at the position of the three sources and a consistent upper-limit with *Chandra* was found. Note that the two DCBH candidates selected by Pacucci et al. (2016) are strong detections, with a full-band X-ray flux of $\sim 6 - 7 \times 10^{-16} \text{ erg s}^{-1} \text{ cm}^{-2}$, calculated from 125 counts.

5. Discussion and Conclusions

In the present study, we conducted an observational search for DCBHs, which represent one of the proposed mechanisms for the formation of supermassive black holes. This scenario elucidates the process by which black holes achieve masses exceeding $10^9 M_{\odot}$ during the early stages of the Universe. Fortunately,

Table 1. List of the selected sources and the corresponding best-fit parameters obtained with the $z > 6$ DCBH models (Pacucci et al. 2016).

Parameters/ObsID ^a	DCBH-1	DCBH-2	DCBH-3
RA(deg)	260.75396245	260.69140947	260.76023184
Dec(deg)	+65.80118827	+65.79172734	+65.82216607
F090W	–	29.59±1.62	28.60±0.88
F115W	–	28.57±0.62	–
F150W	–	27.43±0.19	25.86±0.10
F200W	29.91±0.79	26.55±0.10 ^b	24.61±0.10
F277W	28.83±0.15	25.46±0.10	23.65±0.10
F356W	28.42±0.10	24.71±0.10	22.98±0.10
F410M	27.95±0.13	24.48±0.10	22.68±0.10
F444W	27.50±0.10	24.24±0.10	22.56±0.10
Redshift	14.1	8.2	6.8
$\log_{10}(M/M_{\odot})$	5.56	6.18	6.53
χ^2_{ν}	2.41	0.53	2.48

Notes. ^aObservation ID based on the combined NEP1 and NEP2 catalog. ^bError bars smaller than 0.1 mag were set to 0.1 mag.**Fig. 5.** Detection limits on the number density of halos that may host DCBHs as a function of redshift. The light grey region represents the approximate range of theoretical predictions of the comoving number densities of halos that may host DCBHs, based on Habouzit et al. (2016b). The red lines represent the lowest detectable host halo comoving density in the case of a DCBHs that remains sufficiently bright for detection in at least four JWST/NIRCam filters and retains their characteristic spectral signatures for 10 Myr, given the total survey areas of PEARLS NEP (4 spokes; solid red line), CEERS (dashed red) and JADES (dotted red). The part of parameter space ruled out by the current limit derived in this paper is marked by the dark grey region. The black dashed line represents the approximate $z = 6$ quasar number density, which DCBH models must exceed prior to these redshifts to explain the SMBH powering these objects.

with the launch of JWST, we now possess the capability to explore the depths of high redshifts and low luminosities, enabling us to delve into the past and investigate this phenomenon with unprecedented precision in the IR regime.

As we have shown, objects with photometric SEDs that closely resemble the Pacucci et al. (2016) predictions of $z \gtrsim 6$ DCBHs do exist, even in full 8-band JWST/NIRCam data sets of the type provided by the PEARLS/NEP survey. Since a DCBH

sample selected in this way may include heavily dust-reddened galaxies and AGN (see Sect. 3), additional data are required to ascertain the true nature of these objects.

The spectroscopic signatures of the DCBH models by Pacucci et al. (2016) include very strong hydrogen Balmer lines, an $H\alpha/H\beta$ emission-line ratio of $H\alpha/H\beta > 10$ (i.e., in significant excess of the case B recombination value of ≈ 2.8 due to collisional pumping of $H\alpha$), a strong $\text{HeII}1640$ emission line, and an absence of emission lines due to metals (Pacucci et al. 2017b). At $z \gtrsim 6.9$, $H\alpha$ redshifts out of JWST/NIRSpec wavelength range, but remains within reach of JWST/MIRI imaging and spectroscopy until $z \approx 15$. Follow-up observations with NIRSpec and MIRI could therefore rule out both dusty starbursts and AGN, at least for the brightest of our candidates.

If the DCBH is located inside a large ionized bubble in the intergalactic medium (for instance because the formation of the DCBH has been triggered by a nearby AGN; e.g., Johnson & Aykutalp 2019), the $\text{Ly}\alpha$ line could also be partially transmitted. However, the transmission of a significant $\text{Ly}\alpha$ flux at $z \gtrsim 6$ would alter the photometric signature (e.g., Zackrisson et al. 2011a), and the selection made here and by Pacucci et al. (2016) was made assuming a negligible $\text{Ly}\alpha$ contribution to the SED.

Due to stochastic gas accretion onto the black hole, DCBHs may also display brightness variations (Wang et al. 2017), thus standing out in multi-epoch observations with NIRCam. While this makes DCBHs distinct from dusty galaxies (except in the rare case of a supernova going off in a star-forming galaxy), it does not, however, effectively separate DCBH from AGN.

The extended morphology, evident in some of our candidates, could arise from ionized gas around the DCBH, as shown in some early simulations. However, the morphological structure would be nearly spherical in this case, with a typical radius of 0.5 kpc (see, e.g., Latif et al. 2013). If the extended structure is not associated with the central DCBH, it must be caused either by the DCBH host galaxy or a nearby galaxy. However, an evident stellar component in the candidate’s image would substantially impact the SED, invalidating the use of DCBH models without accounting for the galaxy contribution. Consequently, our current search approach is designed to avoid detecting such objects. This paper focuses on identifying the “pure” (or nearly pure) DCBH scenario.

Acknowledgements. AN and EZ acknowledge funding from Olle Engkvists Stiftelse. EZ also acknowledges funding from the Swedish National Space Agency

and grant 2022-03804 from the Swedish Research Council. WPM acknowledges that the National Aeronautics and Space Administration provided support for this work through Chandra Award Numbers GO8-19119X, GO9-20123X, GO0-21126X, and GO1-22134X issued by the Chandra X-ray Center, which the Smithsonian Astrophysical Observatory operates for and on behalf of the National Aeronautics Space Administration under contract NAS8-03060. FP acknowledges support from a Clay Fellowship administered by the Smithsonian Astrophysical Observatory. This work was also supported by the Black Hole Initiative at Harvard University, which is funded by grants from the John Templeton Foundation and the Gordon and Betty Moore Foundation. This work is also based on observations made with the NASA/ESA/CSA James Webb Space Telescope. The data were obtained from the Mikulski Archive for Space Telescopes at the Space Telescope Science Institute, which is operated by the Association of Universities for Research in Astronomy, Inc., under NASA contract NAS 5-03127 for JWST. These observations are associated with JWST programs 1176 and 2738. RAW, SHC, and RAJ acknowledge support from NASA JWST Interdisciplinary Scientist grants NAG5-12460, NNX14AN10G, and 80NSSC18K0200 from GSFC. Work by CJC and NJA acknowledge support from the European Research Council (ERC) Advanced Investigator Grant EPOCHS (788113). BLF thanks the Berkeley Center for Theoretical Physics for their hospitality during the writing of this paper. MAM acknowledges the support of a National Research Council of Canada Plaskett Fellowship, and the Australian Research Council Centre of Excellence for All Sky Astrophysics in 3 Dimensions (ASTRO 3D), through project number CE17010001. CNAW acknowledges funding from the JWST/NIRCam contract NASS-0215 to the University of Arizona. AZ acknowledges support by Grant No. 2020750 from the United States-Israel Binational Science Foundation (BSF) and Grant No. 2109066 from the United States National Science Foundation (NSF), and by the Ministry of Science & Technology, Israel. We also acknowledge the indigenous peoples of Arizona, including the Akimel O'odham (Pima) and Pee Posh (Maricopa) Indian Communities, whose care and keeping of the land has enabled us to be at ASU's Tempe campus in the Salt River Valley, where much of our work was conducted.

References

- Algera, H. S. B., Inami, H., Oesch, P. A., et al. 2023, *MNRAS*, 518, 6142
- Aykutalp, A., Barrow, K. S. S., Wise, J. H., & Johnson, J. L. 2020, *ApJ*, 898, L53
- Aykutalp, A., Wise, J. H., Spaans, M., & Meijerink, R. 2014, *ApJ*, 797, 139
- Bañados, E., Venemans, B. P., Mazzucchelli, C., et al. 2018, *Nature*, 553, 473
- Baraffe, I., Homeier, D., Allard, F., & Chabrier, G. 2015, *A&A*, 577, A42
- Barro, G., Perez-Gonzalez, P. G., Kocevski, D. D., et al. 2023, arXiv e-prints, arXiv:2305.14418
- Barrow, K. S. S., Aykutalp, A., & Wise, J. H. 2018, *Nature Astronomy*, 2, 987
- Barrufet, L., Oesch, P. A., Weibel, A., et al. 2023, *MNRAS*, 522, 449
- Begelman, M. C. 1978, *MNRAS*, 184, 53
- Begelman, M. C. & Volonteri, M. 2017, *MNRAS*, 464, 1102
- Bertin, E. & Arnouts, S. 1996, *A&AS*, 117, 393
- Boekholt, T. C. N., Schleicher, D. R. G., Fellhauer, M., et al. 2018, *MNRAS*, 476, 366
- Bromm, V. & Loeb, A. 2003, *ApJ*, 596, 34
- Carnall, A. C., McLure, R. J., Dunlop, J. S., & Davé, R. 2018, *MNRAS*, 480, 4379
- Davies, M. B., Miller, M. C., & Bellovary, J. M. 2011, *ApJ*, 740, L42
- Eisenstein, D. J., Willott, C., Alberts, S., et al. 2023, arXiv e-prints, arXiv:2306.02465
- Fan, X., Banados, E., & Simcoe, R. A. 2022, arXiv e-prints, arXiv:2212.06907
- Fan, X., Strauss, M. A., Schneider, D. P., et al. 2003, *AJ*, 125, 1649
- Fan, X., et al. 2001, *AJ*, 122, 2833
- Ferrara, A., Salvadori, S., Yue, B., & Schleicher, D. 2014, *MNRAS*, 443, 2410
- Finkelstein, S. L., Bagley, M. B., Haro, P. A., et al. 2022, *ApJ*, 940, L55
- Furtak, L. J., Zitrit, A., Plat, A., et al. 2022, arXiv e-prints, arXiv:2212.10531
- Habouzit, M., Volonteri, M., Latif, M., Dubois, Y., & Peirani, S. 2016a, *MNRAS*, 463, 529
- Habouzit, M., Volonteri, M., Latif, M., Dubois, Y., & Peirani, S. 2016b, *MNRAS*, 463, 529
- Hasinger, G. 2020, *J. Cosmology Astropart. Phys.*, 2020, 022
- Inayoshi, K., Onoue, M., Sugahara, Y., Inoue, A. K., & Ho, L. C. 2022a, *ApJ*, 931, L25
- Inayoshi, K., Onoue, M., Sugahara, Y., Inoue, A. K., & Ho, L. C. 2022b, *ApJ*, 931, L25
- Inayoshi, K., Visbal, E., & Haiman, Z. 2020, *ARA&A*, 58, 27
- Jansen, R. A. & Windhorst, R. A. 2018, *PASP*, 130, 124001
- Johnson, J. L. & Aykutalp, A. 2019, *ApJ*, 879, 18
- Katz, H., Sijacki, D., & Haehnelt, M. G. 2015, *MNRAS*, 451, 2352
- Kocevski, D. D., Onoue, M., Inayoshi, K., et al. 2023, arXiv e-prints, arXiv:2302.00012
- Kokorev, V., Jin, S., Magdis, G. E., et al. 2023, *ApJ*, 945, L25
- Labbe, I., Greene, J. E., Bezanson, R., et al. 2023, arXiv e-prints, arXiv:2306.07320
- Larson, R. L., Finkelstein, S. L., Kocevski, D. D., et al. 2023, arXiv e-prints, arXiv:2303.08918
- Latif, M. A., Schleicher, D. R. G., Schmidt, W., & Niemeyer, J. 2013, *MNRAS*, 433, 1607
- Latif, M. A., Whalen, D. J., Khochfar, S., Herrington, N. P., & Woods, T. E. 2022, arXiv e-prints, arXiv:2207.05093
- Lodato, G. & Natarajan, P. 2006, *MNRAS*, 371, 1813
- Loeb, A. & Rasio, F. A. 1994, *ApJ*, 432, 52
- Matthee, J., Naidu, R. P., Brammer, G., et al. 2023, arXiv e-prints, arXiv:2306.05448
- Mortlock, D. J., Warren, S. J., Venemans, B. P., et al. 2011, *Nature*, 474, 616
- Nakajima, K. & Maiolino, R. 2022, *MNRAS*, 513, 5134
- Natarajan, P., Pacucci, F., Ferrara, A., et al. 2017, *ApJ*, 838, 117
- Pacucci, F., Baldassare, V., Cappelluti, N., et al. 2019, *BAAS*, 51, 117
- Pacucci, F., Ferrara, A., Grazian, A., et al. 2016, *MNRAS*, 459, 1432
- Pacucci, F., Ferrara, A., Volonteri, M., & Dubus, G. 2015, *MNRAS*, 454, 3771
- Pacucci, F. & Loeb, A. 2020, *ApJ*, 895, 95
- Pacucci, F. & Loeb, A. 2022, *MNRAS*, 509, 1885
- Pacucci, F., Natarajan, P., Volonteri, M., Cappelluti, N., & Urry, C. M. 2017a, *ApJ*, 850, L42
- Pacucci, F., Pallottini, A., Ferrara, A., & Gallerani, S. 2017b, *MNRAS*, 468, L77
- Phillips, M. W., Tremblin, P., Baraffe, I., et al. 2020, *A&A*, 637, A38
- Polletta, M., Tajer, M., Maraschi, L., et al. 2007, *ApJ*, 663, 81
- Portegies Zwart, S. F. & McMillan, S. L. W. 2002, *ApJ*, 576, 899
- Rieke, M. J., Kelly, D. M., Misselt, K., et al. 2023, *PASP*, 135, 028001
- Rodighiero, G., Bisigello, L., Iani, E., et al. 2023, *MNRAS*, 518, L19
- Smail, I., Dudzeviciute, U., Gurwell, M., et al. 2023, arXiv e-prints, arXiv:2306.16039
- Valiante, R., Agarwal, B., Habouzit, M., & Pezzulli, E. 2017, *PASA*, 34, e031
- Valiante, R., Schneider, R., Zappacosta, L., et al. 2018, *MNRAS*, 476, 407
- Visbal, E. & Haiman, Z. 2018, *ApJ*, 865, L9
- Volonteri, M., Habouzit, M., & Colpi, M. 2021, *Nature Reviews Physics*, 3, 732
- Wang, F., Yang, J., Fan, X., et al. 2021, *ApJ*, 907, L1
- Wang, L., Baade, D., Baron, E., et al. 2017, arXiv e-prints, arXiv:1710.07005
- Whalen, D. J., Surace, M., Bernhardt, C., et al. 2020, *ApJ*, 897, L16
- Windhorst, R. A., Cohen, S. H., Jansen, R. A., et al. 2023, *AJ*, 165, 13
- Woods, T. E., Agarwal, B., Bromm, V., et al. 2019, *PASA*, 36, e027
- Wu, X.-B., Wang, F., Fan, X., et al. 2015, *Nature*, 518, 512
- Wyithe, J. S. B. & Loeb, A. 2012, *MNRAS*, 425, 2892
- Yang, J., Wang, F., Fan, X., et al. 2020, *ApJ*, 897, L14
- Zackrisson, E., Inoue, A. K., Rydberg, C.-E., & Duval, F. 2011a, *MNRAS*, 418, L104
- Zackrisson, E., Rydberg, C.-E., Schaerer, D., Östlin, G., & Tuli, M. 2011b, *ApJ*, 740, 13
- Zhao, X., Civano, F., Fornasini, F. M., et al. 2021, *MNRAS*, 508, 5176

Appendix A: Properties of galaxies with the potential to mimic the SEDs of DCBHs

Here, we provide additional constraints on the properties of galaxies capable of mimicking the photometric signatures of DCBHs. By treating the [Pacucci et al. \(2016\)](#) DCBH SED models as mock observations and attaching realistic observational errorbars to the resulting NIRCam photometric data points, we used the BAGPIPES code ([Carnall et al. 2018](#)) to fit galaxy models to these data. We found that the mock NIRCam photometry can be reproduced by galaxies with dust attenuation of $A_V \gtrsim 2$ mag over a wide range of redshifts.

Fig. A.1 presents two cases where mock NIRCam data generated from DCBH models at $z_{\text{DCBH}} = 6$ (a) and $z_{\text{DCBH}} = 12$ (b) DCBH are fitted by models involving highly dust-reddened stellar populations. The first case involves a dusty stellar population at a redshift similar to that of the DCBH model, while the second case involves a dusty galaxy at a significantly lower redshift of $z \approx 4$. It is also possible to find solutions in which the best-fitting galaxy models have redshifts higher than those of the underlying DCBH models. However, since this requires extremely dusty galaxies forming very early in the history of the Universe, such interlopers should be considerably less common ([Algera et al. 2023](#)), and medium-band filters are also effective at removing dusty galaxies.

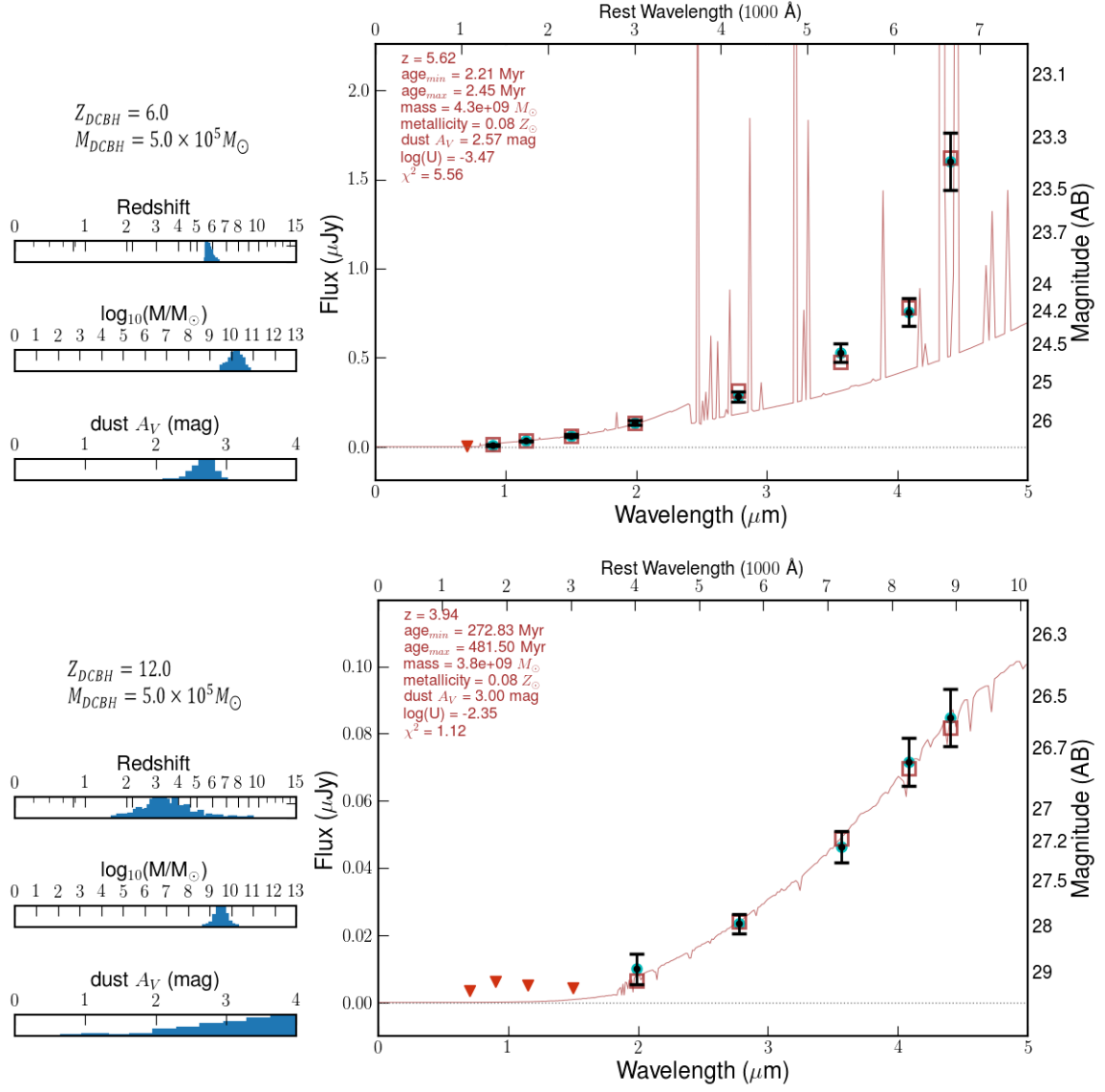


Fig. A.1. BAGPIPES fits of galaxy models to mock DCBH data. The red squares represent the best-fitting galaxy model, based on the red model galaxy spectrum, to the photometric fluxes of $M_{\text{DCBH}} = 5 \times 10^5 M_{\odot}$ DCBH model (black circles with mock error bars) from [Pacucci et al. \(2016\)](#). Red triangles indicate filters where the mock DCBH fluxes fall below the PEARLS detection limits of the NEP field. The estimated errors on the fitted redshift, total stellar mass, and dust attenuation of the galactic fit are indicated by the sliders to the left of each plot. *Top*: Example where a $z_{\text{DCBH}} = 6$ spectrum is fitted by a dusty galaxy model at a similar redshift ($z \approx 5.62$). *Bottom*: Example where a $z_{\text{DCBH}} = 12$ spectrum is fitted by a dusty galaxy model at a significantly lower redshift ($z \approx 3.94$).